



Distinctive phosphoinositide- and Ca²⁺-binding properties of normal and cognitive performance-linked variant forms of KIBRA C2 domain

Received for publication, February 5, 2018, and in revised form, May 3, 2018. Published, Papers in Press, May 3, 2018, DOI 10.1074/jbc.RA118.002279

Mareike G. Posner[‡], Abhishek Upadhyay[‡], Rieko Ishima[§], Antreas C. Kalli[¶], Gemma Harris^{**}, Joachim Kremerskothen^{††}, Mark S. P. Sansom^{§§}, Susan J. Crennell[‡], and  Stefan Bagby^{‡1}

From the [‡]Department of Biology and Biochemistry, University of Bath, Bath BA2 7AY, United Kingdom, [§]Department of Structural Biology, University of Pittsburgh School of Medicine, Pittsburgh, Pennsylvania 15260, [¶]Leeds Institute of Cancer and Pathology, University of Leeds, Leeds LS9 7TF, United Kingdom, ^{||}Astbury Centre for Structural Molecular Biology, University of Leeds, Leeds LS2 9JT, United Kingdom, ^{**}Research Complex at Harwell, Rutherford Appleton Laboratory, Didcot OX11 0FA, United Kingdom, ^{††}Internal Medicine D, Department of Nephrology, Hypertension and Rheumatology, University Hospital Münster, D-48149 Münster, Germany, and ^{§§}Department of Biochemistry, University of Oxford, Oxford OX1 3QU, United Kingdom

Edited by Wolfgang Peti

Kidney- and brain-expressed protein (KIBRA), a multifunctional scaffold protein with around 20 known binding partners, is involved in memory and cognition, organ size control via the Hippo pathway, cell polarity, and membrane trafficking. KIBRA includes tandem N-terminal WW domains, a C2 domain, and motifs for binding atypical PKC and PDZ domains. A naturally occurring human KIBRA variant involving residue changes at positions 734 (Met-to-Ile) and 735 (Ser-to-Ala) within the C2 domain affects cognitive performance. We have elucidated 3D structures and calcium- and phosphoinositide-binding properties of human KIBRA C2 domain. Both WT and variant C2 adopt a canonical type I topology C2 domain fold. Neither Ca²⁺ nor any other metal ion was bound to WT or variant KIBRA C2 in crystal structures, and Ca²⁺ titration produced no significant reproducible changes in NMR spectra. NMR and X-ray diffraction data indicate that KIBRA C2 binds phosphoinositides via an atypical site involving β -strands 5, 2, 1, and 8. Molecular dynamics simulations indicate that KIBRA C2 interacts with membranes via primary and secondary sites on the same domain face as the experimentally identified phosphoinositide-binding site. Our results indicate that KIBRA C2 domain association with membranes is calcium-independent and involves distinctive C2 domain–membrane relative orientations.

Kidney- and brain-expressed protein (KIBRA²; also called WW- and C2 domain–containing protein 1 (WWC1)) is a large

This work was supported by Biotechnology and Biological Sciences Research Council Grant BB/J008176/1. The authors declare that they have no conflicts of interest with the contents of this article.

This article contains Figs. S1–S9 and Tables S1–S4.

The atomic coordinates and structure factors (codes 6FB4, 6FD0, 6FJD, and 6FJC) have been deposited in the Protein Data Bank (<http://www.pdb.org/>).

NMR chemical shift data have been deposited in the Biological Magnetic Resonance Bank (BMRB) under accession numbers 27429 and 27430.

¹ To whom correspondence should be addressed. Tel.: 44-1225-386436; Fax: 44-1225-386779; E-mail: bsssb@bath.ac.uk.

² The abbreviations used are: KIBRA, kidney- and brain-expressed protein; AD, Alzheimer's disease; AUC, analytical ultracentrifugation; CBR, calcium-binding region; MD, molecular dynamics; C2(C771A), C771A mutant of KIBRA C2 domain; PI(3)P, phosphatidylinositol 3-phosphate; PI(4,5)P₂,

(1119-, 1118-, and 1113-amino acid isoforms), multifunctional scaffold protein that has two N-terminal WW domains, a putative nuclear localization signal (1), putative coiled-coil regions, a C2 domain, a glutamic acid-rich motif, an atypical PKC-binding region, and a C-terminal PDZ-binding motif (see Fig. 1). KIBRA has about 20 reported binding partners (2) and disease links, including dementia (3–5), kidney disease (6), Tourette disorder (7), and some cancers (8, 9). Among its multiple functions, KIBRA is an upstream component of the Hippo pathway (8, 10), a central mechanism of organ size control and cellular homeostasis. KIBRA also has a role in cell polarity and migration, functioning as a link between polarity proteins and cytoskeleton components (2, 11–14). In addition, KIBRA functions in membrane trafficking via regulation of vesicular transport (12, 15–17).

KIBRA is linked to memory, cognition, and neurological disorders in humans and in rodent models (for a review, see Ref. 2). A single nucleotide polymorphism (SNP), rs17070145, in the ninth intron of KIBRA, for example, has been implicated in human cognition (15), a finding corroborated by numerous subsequent studies, including a meta-analysis (16). rs17070145 is associated with Alzheimer's disease (AD) (3, 17). KIBRA, moreover, has additive and epistatic interactions with APOE (18), the $\epsilon 4$ allele of which is the strongest genetic risk factor for sporadic AD. The effect of SNP rs17070145 on memory and AD may arise due to differential activation of the MAPK pathway (19), important for memory and learning processes. In human, rat, and mouse brains, KIBRA is mainly expressed in memory-related regions, including hippocampus and cortex, as well as cerebellum and hypothalamus (15, 20, 21).

KIBRA acts in the same pathway as protein kinase M ζ (PKM ζ), a brain-specific kinase thought to be involved in long-

phosphatidylinositol 4,5-bisphosphate; PI(3,4,5)P₃, phosphatidylinositol 3,4,5-trisphosphate; r.m.s.d., root mean square deviation; varC2, naturally occurring variant (M734I,S735A) KIBRA C2 domain; varC2(C771A), C771A mutant of variant KIBRA C2 domain; WTC2, wildtype KIBRA C2 domain; WWC, WW- and C2 domain–containing protein; XRC, X-ray crystallography; PKM ζ , protein kinase M ζ ; HSQC, heteronuclear single quantum coherence; CG-MD, coarse-grained molecular dynamics.

KIBRA C2: Distinctive phosphoinositide and Ca²⁺ binding

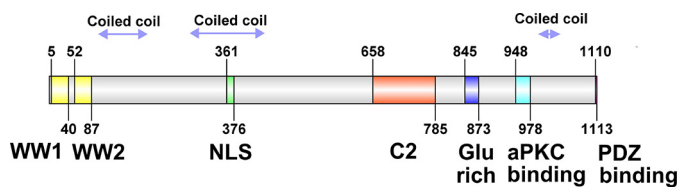


Figure 1. Schematic structure of human KIBRA protein showing locations of motifs and domains. The nuclear localization signal (NLS) and coiled-coil regions are predicted rather than experimentally demonstrated. *aPKC*, atypical PKC.

term memory storage through its control of neuroreceptor trafficking, particularly trafficking of α -amino-3-hydroxy-5-methyl-4-isoxazolepropionic acid (AMPA) receptors, the major excitatory neurotransmitter receptors in the brain (22). KIBRA binds, colocalizes with, and is phosphorylated by PKM ζ (11, 23), and KIBRA is involved in AMPA receptor trafficking (24). KIBRA counteracts proteasomal degradation of PKM ζ (25). In addition, KIBRA binds to dendrin (26) and synaptopodin (13, 27), postsynaptic cytoskeleton organizers important for synaptic transmission and cognition. Aberrant acetylation of tau, linked to cognitive deterioration in dementia, disrupts postsynaptic function by reducing postsynaptic KIBRA (4, 28). Consistent with these accumulated observations, KIBRA overexpression and knockdown exert positive and negative effects, respectively, on key molecular and cellular processes in neurons (29). It has been shown by immunoprecipitation that KIBRA can form homodimers (20) and heterodimers with the two other WWC protein family members, WWC2 and WWC3 (10), although the functional significance of this remains unknown.

Here, we characterize the calcium- and phosphoinositide-binding properties of KIBRA C2 domain (Fig. 1), including a variant that arises from two SNPs (rs3822660G/T and rs3822659T/G) in human KIBRA that result in substitution of two adjacent residues (M734I,S735A) (30). Although the molecular consequences of these exonic SNPs have not been fully elucidated, they affect cognitive performance, and there is almost complete linkage disequilibrium between the aforementioned intronic SNP rs17070145 (15) and rs3822660G/T and rs3822659T/G (30).

The C2 domain is found in more than 125 different human proteins (31, 32). Although most C2 domains are Ca²⁺-dependent membrane association domains, some C2 domains do not bind Ca²⁺, and some mediate protein–protein rather than protein–lipid interactions (31, 32). Our experimental and computational investigations of WT and variant KIBRA C2 domains indicate that KIBRA C2 is a noncanonical C2 domain that *in vitro* both binds phosphoinositides and associates with membranes in an atypical, calcium-independent manner.

Results

WT and variant KIBRA C2 adopt a typical C2 fold

Our 2.6-Å resolution crystal structure (Protein Data Bank code 6FD0) shows that variant C2 (varC2) adopts a typical eight-stranded β -sandwich C2 domain fold. The crystal form comprises a parallel dimer (*i.e.* the two monomers are parallel to each other) formed via an intermonomer disulfide bond involving Cys-771, the fifth and only unpaired cysteine in

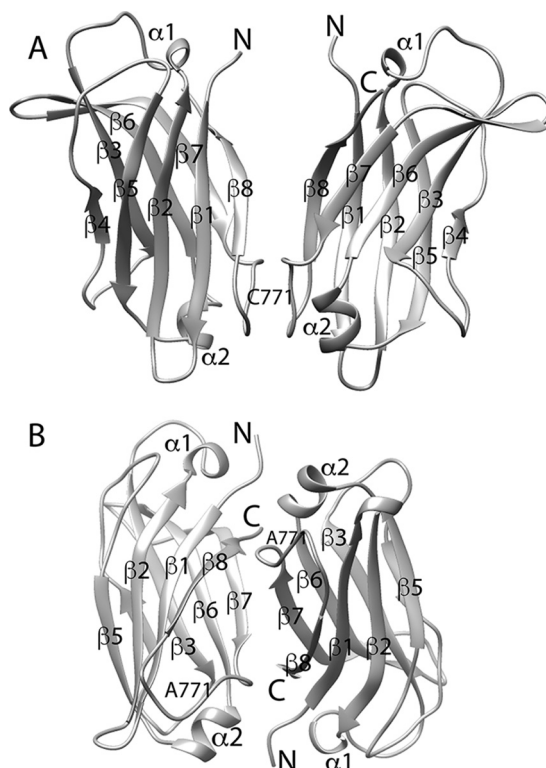


Figure 2. Crystal structures of variant and mutant (C771A) KIBRA C2. A, varC2 parallel dimer (Protein Data Bank code 6FD0). B, C2(C771A) antiparallel dimer (Protein Data Bank code 6FB4). Termini, β -strands, α -helices, and residue 771 are labeled. In A, the Cys-771 label corresponds to the position of the intermonomer disulfide bond, which mediates parallel dimer formation in the WTC2 and varC2 crystal structures.

KIBRA C2 (Fig. 2A). The previously available crystal structure of WT KIBRA C2 (Protein Data Bank code 2Z0U) involves a similar parallel, Cys-771 disulfide-linked dimer. According to analytical ultracentrifugation (AUC) measurements (Fig. S1 and Table S2), WTC2 and varC2 samples both comprise a mixture of monomer and dimer in solution.

Conversely, AUC and nuclear magnetic resonance (NMR) relaxation measurements (Figs. S1 and S2 and Tables S2 and S3) indicate that the C771A mutant C2 (C2(C771A)) and variant C771A mutant C2 (varC2(C771A)) are monomeric in solution. NMR samples of C2(C771A) and varC2(C771A) were homogeneous and stable, permitting backbone resonance assignments to be made using standard NMR methods (Fig. S3). Although AUC and NMR indicate that C2(C771A) is monomeric in solution, its crystal structure (Protein Data Bank code 6FB4; 2.5-Å resolution) comprises an antiparallel dimer (Fig. 2B), most likely formed due to crystal packing.

The backbone ¹H, ¹³C, and ¹⁵N NMR chemical shifts of C2(C771A) and varC2(C771A) match closely the corresponding chemical shifts back-calculated using SPARTA+ (33) from the C2(C771A) crystal structure (Protein Data Bank code 6FB4). Correspondingly, the TALOS+ (34) and SPARTA+ (33) predictions are that the secondary structure compositions of C2(C771A) and varC2(C771A) in solution are very similar to the C2(C771A) crystal structure (Fig. S4). The β -sheet NOE patterns of C2(C771A) and varC2(C771A), moreover, are as expected based on the C2 topology I fold, allowing for peak overlap and absence. NMR data therefore indicate that

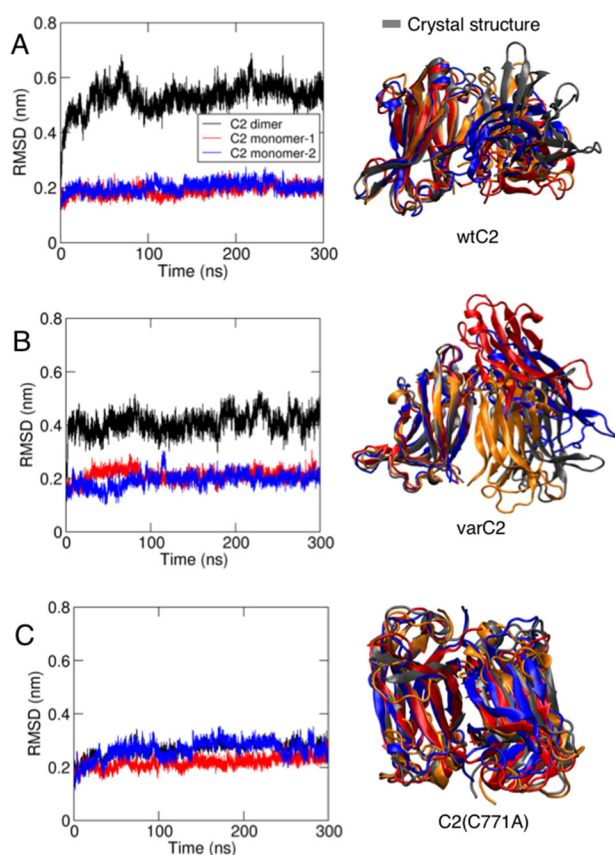


Figure 3. MD simulation of KIBRA C2 dimer conformation in solution. r.m.s.d. for WTC2 (A), varC2 (B), and varC2(C771A) (C) with r.m.s.d. for the monomers in blue and red and for the dimer in black is shown for one of the simulations of each system. Final structures from the three repeat simulations for each system are also shown with one monomer superimposed, in blue, red, and orange, with the corresponding crystal structure in gray.

C2(C771A) and varC2(C771A) in solution are conformationally very similar to each other (Fig. S5) and to C2 monomers in C2(C771A), varC2 (Protein Data Bank codes 6FB4 and 6FD0, respectively) and WTC2 (Protein Data Bank code 2Z0U) crystal structures.

Because KIBRA dimerization has been indicated by cell-based data (10, 20), MD simulations were conducted to compare conformational stabilities of the C2 dimers observed in crystal structures. Both parallel dimers (WTC2/2Z0U and varC2/6FD0) exhibited significant changes in relative monomer position (Fig. 3) with the changes varying between repeat simulations and force fields. In WTC2 dimer simulations, the mean r.m.s.d. value after three repeat simulations was 0.52 ± 0.04 and 0.49 ± 0.05 nm for GROMOS and OPLS force fields, respectively. The corresponding values in varC2 simulations were 0.51 ± 0.08 nm and 1.4 ± 0.23 nm. In equivalent simulations, in contrast, the C2(C771A) antiparallel dimer (Protein Data Bank code 6FB4) did not undergo significant changes in relative monomer position. There were no significant conformational changes within C2 monomers in any simulation (Fig. 3).

NMR and X-ray diffraction data indicate that KIBRA C2–Ca²⁺ interaction is very low-affinity and nonspecific

Ca²⁺ binding was investigated by NMR, X-ray crystallography (XRC), and simulation. In numerous ¹H-¹⁵N HSQC-mon-

itored titrations with C2(C771A) and one with WTC2, calcium chloride addition to 10–20 mM and sometimes higher concentrations (up to 76 mM) produced no significant reproducible chemical shift change with the largest composite ¹H-¹⁵N changes around 0.05 ppm. Such small changes may be due to a very weak Ca²⁺ ion interaction ($K_d > 10$ mM), possibly nonspecific Ca²⁺ binding to oxygen-rich surface clusters. Such a nonspecific interaction is supported by simulation: when eight Ca²⁺ ions were initially positioned randomly around KIBRA C2, the final Ca²⁺ positions in eight simulations included the calcium-binding regions (CBRs) plus six other locations around the domain (Fig. S6).

It is also possible that the domain scavenged Ca²⁺ during expression and purification and was therefore Ca²⁺-bound prior to the experiments, although this seems unlikely because particular effort was made during some C2 NMR sample preparations to exclude Ca²⁺. Initial ¹H-¹⁵N HSQC spectra were very similar, furthermore, irrespective of whether or not measures were taken to exclude Ca²⁺ from NMR samples.

In several crystal structures, including WTC2 (Protein Data Bank code 2Z0U) and our C2(C771A) and varC2 structures, no bound Ca²⁺ has been observed, although the protein for 2Z0U was produced by cell-free synthesis and Protein Data Bank entry for 2Z0U does not mention any attempt to introduce metal ions. The crystal structures determined here used *Escherichia coli*-expressed protein with no attempt to exclude Ca²⁺, however, so the C2 domains presumably encountered Ca²⁺ and other divalent metal ions during expression and purification. Several times C2 crystals were soaked in solutions containing divalent metal ions, including 20 mM CaCl₂, 100 mM CaCl₂, and 100 mM MnSO₄. Soaking did not cause visible disintegration of the crystals. Diffraction after soaking was still good, but these experiments yielded only one metal-bound structure, which had one Ca²⁺ located in the intermonomer interface of a C2 dimer rather than in any of the CBRs.

Overall, our NMR and XRC data are consistent with KIBRA C2 domain having very low ($K_d > 10$ mM), nonspecific affinity for Ca²⁺. Together with Protein Data Bank code 2Z0U, moreover, our NMR and XRC data show that lack of bound Ca²⁺ does not disrupt KIBRA C2 from adopting a typical C2 domain fold.

KIBRA C2 exhibits an unusual phosphoinositide interaction mode

NMR and XRC studies were conducted to define the phosphoinositide-binding site location(s) on KIBRA C2. Three NMR titrations were conducted by recording ¹H-¹⁵N HSQC spectra as a function of increasing concentration of phosphoinositide and subsequently calcium chloride. These titrations, involving C2(C771A) with phosphatidylinositol 3-phosphate (PI(3)P), C2(C771A) with phosphatidylinositol 4,5-bisphosphate (PI(4,5)P₂), and varC2 with PI(4,5)P₂, produced very similar results in which phosphoinositide-induced chemical shift changes were observed for numerous peaks, almost all located in the β -sheet comprising β -strands 5, 2, 1, and 8 (Fig. 4). Leu-666 (β 1), Ile-677 (β 2), and Leu-678 (β 2) backbone ¹H-¹⁵N peaks exhibited the largest chemical shift perturbations with changes observed for around 20 further backbone ¹H-¹⁵N

KIBRA C2: Distinctive phosphoinositide and Ca²⁺ binding

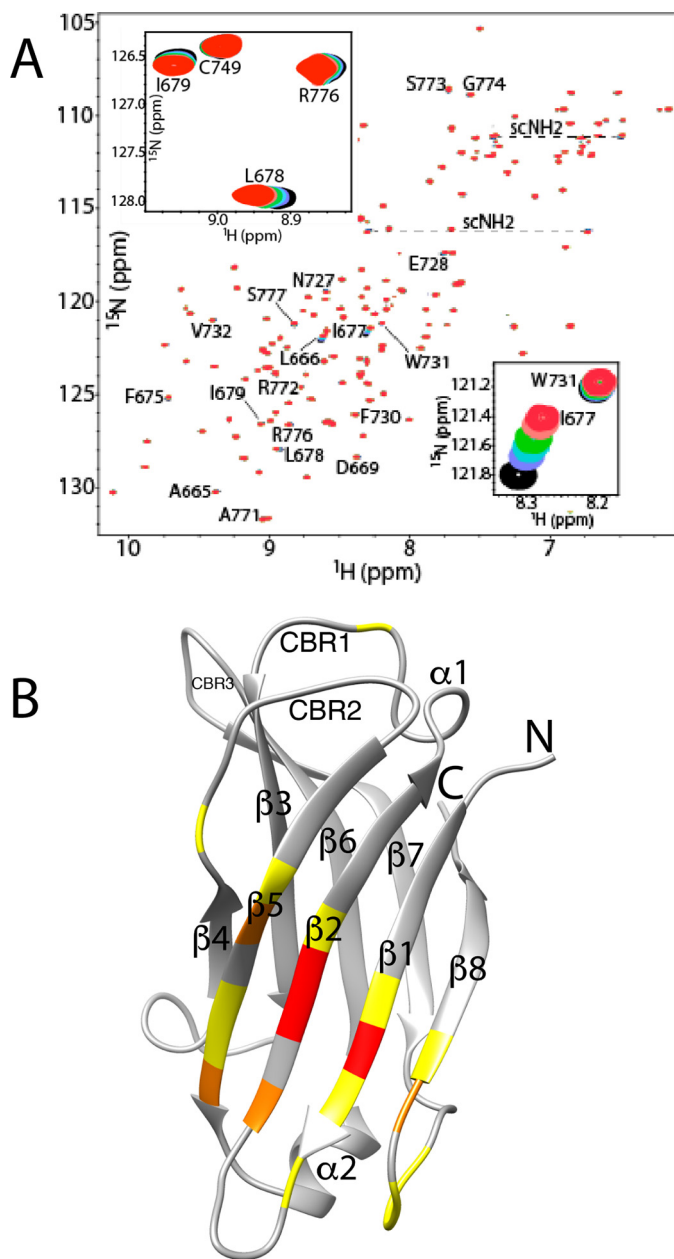


Figure 4. C2(C771A)–PI(3)P interaction monitored by NMR. A, overlay of C2(C771A) ¹H-¹⁵N HSQC spectra as a function of increasing PI(3)P concentration. Perturbed backbone NH peaks are labeled, and the two perturbed but unassigned side-chain NH₂ peak pairs are connected by *dashed lines* and denoted as “scNH₂.” The *insets* highlight the chemical shift changes of backbone NH peaks of Ile-677 (strand β₂) and Trp-731 (β₅) and of Leu-678 (β₂), Ile-679 (β₂), and Arg-776 (β₇-β₈ loop). Peak colors and corresponding C2(C771A):PI(3)P ratios are as follows: red, 1:0; pink, 1:0.25; green, 1:0.5; cyan, 1:0.75; purple, 1:1; black, 1:1.5. B, perturbed residues mapped onto a ribbon representation of C2(C771A). Yellow represents residues with $\Delta\delta_{av}$ (ppm) ≤ 0.01 , orange represents 0.01–0.03, and red represents >0.03 where $\Delta\delta_{av}$ (ppm) = $(\Delta\delta_H^2 + \Delta\delta_N^2(\gamma_N/\gamma_H))/2^{0.5}$. The secondary structure elements (β-strands and α-helices) are labeled. Also, for ease of comparison with other C2 domains, the locations of canonical CBR1, CBR2, and CBR3 are indicated.

peaks plus two pairs of unassigned side-chain NH₂ peaks (Fig. 4). The K_d for C2(C771A)–PI(3)P binding was determined as a representative case using 13 perturbed residues (Fig. S7); the average K_d was 1 mM. After phosphoinositide titration, CaCl₂ was titrated into the same NMR samples to establish whether Ca²⁺ ions influence C2–phosphoinositide interaction or vice

versa; there was no further spectral change upon CaCl₂ addition.

Cocrystallization experiments involving C2(C771A) and varC2 with PI(4,5)P₂ or phosphatidylinositol 3,4,5-trisphosphate (PI(3,4,5)P₃) yielded crystals of C2(C771A) with bound PI(4,5)P₂ and PI(3,4,5)P₃ in ProPlex HT-96 condition G1 (Protein Data Bank codes 6FJD and 6FJC; 2.6- and 2.9-Å resolution, respectively). Both PI(4,5)P₂ and PI(3,4,5)P₃ bound to monomer A of an antiparallel C2(C771A) dimer with polar interactions between Arg-776 (β₇-β₈ loop) and negatively charged oxygen atoms of phosphoinositide phosphates (Fig. 5). Leu-678 (β₂) and Val-729 (β₅) side chains and main chains of Leu-666 (β₁) and Ile-677 (β₂) interact with the phosphoinositide inositol/aliphatic chains. The C2(C771A)–PI(4,5)P₂ and C2(C771A)–PI(3,4,5)P₃ crystal structure binding site is consistent with the phosphoinositide-induced spectral changes in the ¹H-¹⁵N HSQC titrations; the backbone NH groups of Leu-666, Ile-677, and Leu-678, for example, showed the largest chemical shift changes. Phosphoinositide binding occurs with small changes in C2 structure, e.g. a typical overall r.m.s.d. of 0.28 Å between unbound and phosphoinositide-bound structures.

Coarse-grained MD simulations were performed to further examine KIBRA C2 monomer and dimer association with phosphoinositides and membranes. In these simulations, which can predict the binding modes of peripheral proteins to model membrane (35, 36), the three experimentally observed forms of KIBRA C2 (monomer, antiparallel dimer, and parallel dimer, all without Ca²⁺) were displaced away from a preformed phosphoinositide-containing bilayer. In the primary (more frequent) binding mode observed with a C2 monomer, C2 interaction with phosphoinositides involves mainly Arg-661, Lys-671, Arg-772, Arg-776, and Arg-779 (Fig. 6), slightly shifted from the crystal structure/NMR titration binding site. In a small number of simulations, the C2–phosphoinositide interaction involves mainly Lys-667 and Arg-776, coincident with the crystal structure/NMR titration binding site (Figs. 4 and 5). The parallel dimer (WTC2/2Z0U) shows two binding modes with one phosphoinositide often located close to the crystal structure/NMR titration binding site (Fig. 7). The antiparallel dimer (C2(C771A)) exhibits a primary binding mode in which the main interactions with the membrane occur via one of the two C2 domains (Fig. 8). In this orientation, a phosphoinositide is observed near the crystal structure/NMR titration binding site. In all cases, KIBRA C2 domain binding to the bilayer causes a degree of phosphoinositide clustering around the domain. Phosphoinositides interact mainly with lysines and arginines that face the bilayer.

Discussion

KIBRA C2 structure

We have elucidated structural and functional characteristics of four forms of KIBRA C2 domain: WT, naturally occurring variant, and C771A mutants of WT and variant. Variant KIBRA, involving two amino acid changes in the C2 domain (M734L,S735A), affects human cognitive performance and is in almost complete linkage disequilibrium (30) with a previously identified intronic SNP that affects cognition (15, 16). WTC2

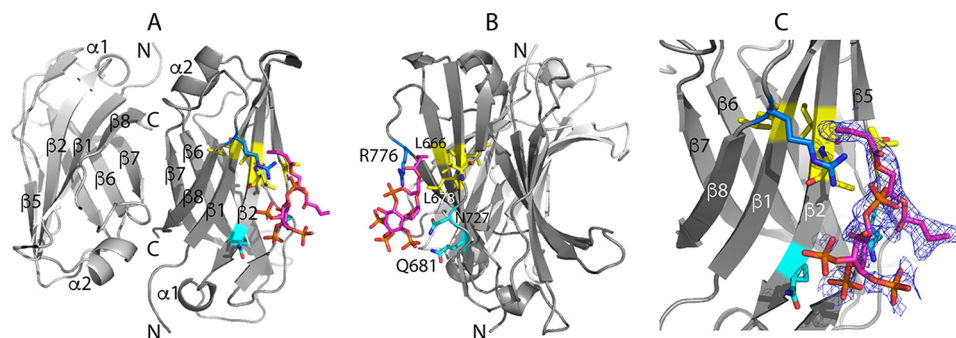


Figure 5. X-ray diffraction structure of the C2(C771A)-PI(3,4,5)P₃ complex. Shown are three views of the complex (Protein Data Bank code 6FJC) in which rotation of view *A* about the vertical axis through $\sim 90^\circ$ gives view *B*. PI(3,4,5)P₃ binds to chain *A* of an antiparallel C2(C771A) dimer as does PI(4,5)P₂. *C*, a closer view of the C2(C771A)-PI(3,4,5)P₃ interaction in the same orientation as *A* with electron density obtained in a simulated annealing omit map around the PI(3,4,5)P₃-binding site shown in *blue mesh*, contoured at 1.1σ . PI(3,4,5)P₃ is shown mainly in *magenta*. Some of the C2 residues that interact with PI(3,4,5)P₃ are shown (hydrophobic residues in *yellow*, polar residues in *cyan*, and positively charged residues in *blue*), including the side chains of Leu-678, Gln-681, Asn-727, and Arg-776 and backbone of Leu-666 and Ile-677. Oxygen and nitrogen atoms are shown in *red* and *dark blue*, respectively.

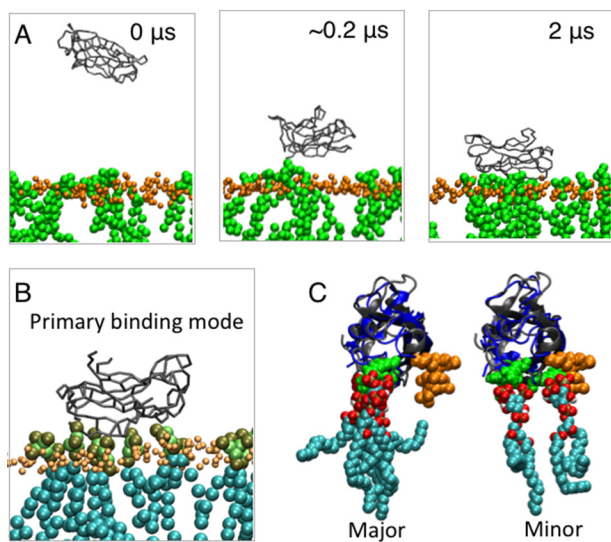


Figure 6. Coarse-grained MD simulation of KIBRA C2 monomer association with membrane. *A*, coarse-grained simulation setup. Snapshots are shown from one of the simulations at 0, ~ 0.2 , and $2 \mu\text{s}$. KIBRA C2 domain is shown in *gray*, lipid phosphate atoms are shown in *orange*, and phosphoinositide lipids are shown in *green*. *B*, a snapshot of one of the simulations showing the preferred orientation of the C2 domain relative to the bilayer. *C*, alignment of C2 domain from the simulations (*gray*) with PI(3,4,5)P₃-bound C2 crystal structure (*blue*). The phosphoinositides bound to C2 in the simulations are also shown. Oxygen atoms on lipids are shown in *red*, hydrogen atoms are shown in *white*, and carbon atoms are shown in *cyan*.

and varC2 adopt a type I topology C2 domain fold with slightly different dimerization properties in solution (Fig. S1), indicating a possible effect of M734I,S735A residue differences on domain behavior. The M734I substitution has previously been calculated to reduce C2 stability (30), although WTC2 and varC2 adopt very similar conformations in both crystal structures and in solution (Figs. S3 and S5).

It has been shown previously that full-length WT KIBRA forms dimers in mammalian cells (20). Overexpression of FLAG-tagged KIBRA in HEK293 cells, moreover, resulted in large KIBRA-containing clusters (20). KIBRA also forms heterodimers with the two other WWC protein family members, WWC2 and WWC3 (10). Yeast two-hybrid mapping indicated that KIBRA dimerizes in an antiparallel orientation with the C2 domain and one or more regions N-terminal of C2 required for this interaction (20). Whether or not KIBRA can dimerize in

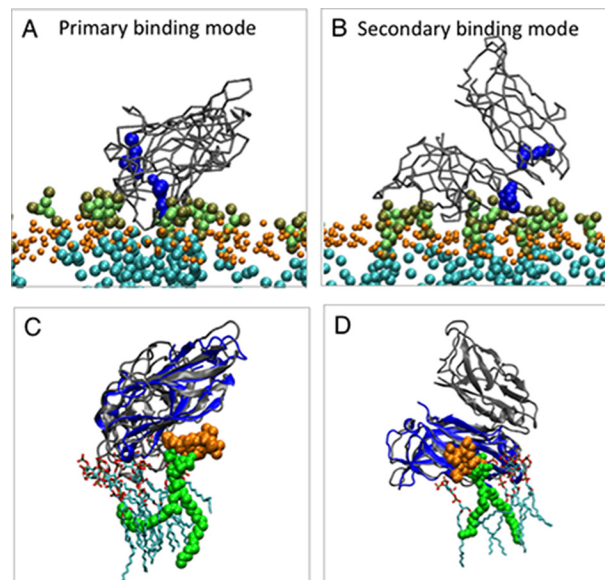


Figure 7. Coarse-grained MD simulation of KIBRA C2 parallel dimer association with membrane. *A* and *B*, primary (*A*) and secondary (*B*) binding modes of the KIBRA C2 parallel dimer from simulation. KIBRA C2 domain is shown in *gray*, lipid phosphate atoms are shown in *orange*, and phosphoinositide lipids are shown in *green*. Residues Lys-667 and Arg-776 are shown in *blue*. *C* and *D*, alignment of C2 domain from the simulations (*gray*) with the PI(3,4,5)P₃-bound C2 crystal structure (*blue*). The phosphoinositides bound to C2 in the simulations are also shown. The phosphoinositide molecule that is close to the phosphoinositide-binding site observed by XRC and NMR is shown in *green*. Oxygen atoms on lipids are shown in *red*, hydrogen atoms are shown in *white*, and carbon atoms are shown in *cyan*.

mammalian cells via intermolecular disulfide bonding remains open to question. Because redox potentials, and therefore likelihood of intermolecular disulfide bonding, vary according to cell type, cell status, and cell compartment, a mixture of non-covalent and covalent WWC protein dimerization modes is possible *in vivo*. The degree of KIBRA dimerization and/or oligomerization in the cell could, for example, fine-tune KIBRA function as a hub for multiprotein complex assembly. Different dimerization tendencies of WTC2 and varC2 could then provide an indication of the molecular mechanism(s) underpinning the link between variant KIBRA C2 and improved cognition (30). Other components of the Hippo pathway are modulated by dimerization; indeed, YAP2L and TAZ form disulfide-mediated dimers that are more stable and more onco-

KIBRA C2: Distinctive phosphoinositide and Ca²⁺ binding

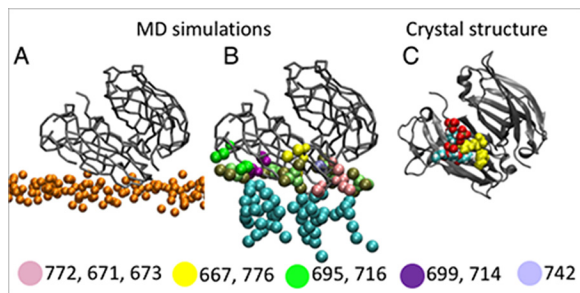


Figure 8. Coarse-grained MD simulation of KIBRA C2 antiparallel dimer association with membrane. *A*, primary orientation of the varC2(C771A) antiparallel dimer relative to the bilayer. The C2 dimer is shown in gray, and lipid phosphate atoms are shown in orange. *B*, phosphoinositide-binding sites on KIBRA C2 resulting from simulation. The residues in each site are shown in a different color. *C*, the varC2(C771A) crystal structure is shown in the same orientation as in *A* and *B*. Residues Lys-667 and Arg-776 that interact with the phosphoinositide analogue are shown as yellow spheres. Oxygen atoms on lipids are shown in red, hydrogen atoms are shown in white, and carbon atoms are shown in cyan.

genic than the corresponding monomers (37). Finally, because oxidative stress can promote disulfide bond formation in cytoplasmic proteins (38), the extent of disulfide-mediated KIBRA dimerization, and hence KIBRA function, could be regulated by oxidative stress. It is potentially relevant in this context that KIBRA-associated pathways can be redox-modulated (39) and that oxidative stress is a hallmark of AD (40).

Calcium binding

Any KIBRA C2–Ca²⁺ interaction is low-affinity ($K_d > 10$ mM): we did not observe bound metal ions in any of our six C2 crystal structures with or without crystal soaking with Ca²⁺ or other divalent metal ions or bound phosphoinositide, and there is no bound Ca²⁺ in the previous WTC2 structure (Protein Data Bank code 2Z0U). In NMR-monitored Ca²⁺ titrations, moreover, the C2(C771A) ¹H–¹⁵N HSQC spectrum did not change significantly. Unlike KIBRA C2, most C2 domains bind Ca²⁺ with sub-mM affinity. For example, synaptotagmin I C2B domain has a Ca²⁺ affinity of about 500 μ M (41), perforin C2 has a Ca²⁺ affinity of \sim 200 μ M (42), and rabphilin-3A C2B domain has a particularly high Ca²⁺ affinity with K_d values of 7 and 11 μ M (43) explained by contributions from C2-flanking residues (44). Like KIBRA C2, however, some C2 domains show very weak or no residual calcium binding; e.g. rat synaptotagmin 4 C2A domain binds Ca²⁺ with a K_d around 10 mM, and rat synaptotagmin 4 C2B domain essentially cannot bind Ca²⁺ despite the lack of an obvious sequence reason (45). The very low Ca²⁺ affinity of KIBRA C2 could at least partly arise from suboptimal sequences for Ca²⁺ binding in CBR1 and CBR3 (Fig. S8).

Phosphoinositide binding and membrane association

C2 domains have been shown to bind phospholipids via the Ca²⁺-binding regions (31, 46) where the phospholipid contributes to the Ca²⁺ coordination sphere. C2 domains also bind phospholipids and phosphoinositides via a β 3– β 4 lysine-rich cluster (31, 47, 48). Our XRC data involving C2(C771A), however, indicate that KIBRA C2 domain binds phosphoinositide in a novel way involving residues from strands β 1, β 2, and β 8 (Fig. 5; Protein Data Bank codes 6FJC and 6FJD). Given this

unusual binding mode, we checked whether C2 dimerization and/or crystal packing hinders phosphoinositide binding at the previously identified C2-phosphoinositide-binding sites: antiparallel C2 domain dimerization with strands β 7 and β 8 forming the intermonomer interface, as observed in our C2(C771A) crystal structures, obscures neither CBRs nor the β 3– β 4 lysine-rich cluster. Similarly, phosphoinositide interaction at the lysine-rich cluster is not prevented by crystal packing: the cluster is not occluded by symmetry-related molecules. Hence, steric factors do not explain why the previously observed phospholipid-binding modes were not observed for KIBRA C2.

Essentially the same phosphoinositide-binding site was also observed in NMR titrations of two phosphoinositides, PI(3)P and PI(4,5)P₂, with C2(C771A) (monomeric), and of PI(4,5)P₂ with varC2 (parallel dimer in crystal structure; Fig. 2), although the binding is relatively low-affinity. The NMR-observed binding involved residues in β 5 as well as β 1, β 2, and β 8 (Fig. 4). Hence, the observed β 1, β 2, β 5, and β 8 phosphoinositide-binding site persisted, irrespective of whether the particular version of KIBRA C2 is predominantly monomer, antiparallel dimer, or parallel dimer.

Possible reasons why phosphoinositide interaction with KIBRA C2 does not occur at previously identified C2 phosphoinositide-binding sites include the fact that KIBRA C2 does not conform to the consensus sequence of the β 3– β 4 lysine-rich cluster (Fig. S9) and may not have sufficient positively charged residues in the vicinity to support phosphoinositide binding. The lack of a lysine-rich cluster may reflect the fact that KIBRA is not required to promote membrane fusion and hence does not need to induce membrane curvature (49). Also, clashes occur when C2(C771A) and PI(4,5)P₂-bound rabphilin 3A structures are overlaid; the side chain of KIBRA residue Glu-757, for example, lies between phosphates 4 and 5 of PI(4,5)P₂ and apparently would repel these phosphate groups of the phosphoinositide; a glutamate occurs at this position in the C2 domains of all three WWC proteins, but an asparagine occurs here in seven of the eight other aligned C2 domains (Fig. S9). In addition, our observation that KIBRA C2 binds calcium very weakly, or perhaps not at all, with consequent lack of electrostatic bridging between KIBRA C2 negatively charged side chains and negatively charged phosphoinositides, helps to explain why phosphoinositide binding is not observed at the CBRs in KIBRA C2. Although the phosphoinositide headgroup is normally expected to be the key moiety, it is also worth considering whether the type of nonpolar tail influences binding: we used diC₄ forms of phosphoinositides for reasonable solubility while retaining an aliphatic tail. Previous C2 studies have used a range of phosphoinositides, including just the PI(4,5)P₂ headgroup (50, 51), diC₈ tails (49), and seemingly full-length tails (47), all resulting in typical C2 phosphoinositide-binding sites. It seems unlikely therefore that phosphoinositide tail type is a significant factor in our observation of an unusual phosphoinositide-binding site in KIBRA C2.

MD simulations indicate that, when associated with membranes, KIBRA C2 can bind to multiple phosphoinositides. As observed for other membrane-bound proteins (52), this results in clustering of phosphoinositide lipids around the protein with

phosphoinositides binding to lysines and arginines that face the membrane. Such phosphoinositide lipid clustering around KIBRA C2 is expected to change the local lipid environment. This, together with the fact that in some simulations we observed secondary orientations of KIBRA C2 relative to the membrane, could influence partner protein recruitment and consequently processes such as trafficking of receptors involved in learning and memory.

In summary, experimental and simulation data indicate that KIBRA C2 is a nonclassical C2 domain that can associate with membranes in a distinctive side-on, Ca²⁺-independent manner. Further investigation is required to tease out the detailed functional significance of this unusual mode of membrane association and consequently its implications for molecular mechanisms of learning and memory, organ size control, and major diseases.

Finally, we caution that we have observed this interaction mode using an isolated C2 domain *in vitro*. Although we have identified several factors that explain the observed binding mode, in the cell it is possible that other factors such as protein-binding partners and membrane composition/structure alter the KIBRA C2–membrane association mode.

Experimental procedures

Cloning, protein expression, and protein purification

Sequences encoding residues 658–785 of WT and variant (M734I/S735A) human KIBRA and C771A mutants of these were PCR-amplified and inserted into pQE30 (Qiagen). Unless otherwise stated, the forms of KIBRA C2 used are as follows: WTC2, varC2, C2(C771A), and varC2(C771A) (details in Table S1). The resulting proteins, with the sequence MRGSHHHH-HHGS N-terminal to Gly-658 of human KIBRA, were expressed using BL21(DE3) with isopropyl 1-thio- β -D-galactopyranoside induction and purified as described previously (53). ¹⁵N- and ¹⁵N/¹³C-labeled C2 domain samples for NMR were produced by expression in M9 minimal medium supplemented with 1 g/liter ¹⁵NH₄Cl as the sole nitrogen source or 1 g/liter ¹⁵NH₄Cl and 2 g/liter [¹³C]glucose as the sole nitrogen and carbon sources, respectively. For NMR and AUC, C2 was exchanged into 10–50 mM MES, pH 6.5, 50–150 mM NaCl. For crystallization screens, C2 was exchanged into 10 mM MES, pH 6.5, 75 mM NaCl.

NMR

NMR data for resonance assignment (Fig. S3) were acquired at 35 °C on a 600-MHz Varian Unity INOVA spectrometer with an ambient temperature probe at University of Bath or on cryoprobe-equipped 700-MHz Bruker or 800-MHz Varian/Agilent spectrometers at the Medical Research Council Biomedical NMR Centre, Mill Hill. Protein concentration used for 3D NMR experiments was in the range 0.5–0.8 mM. NMR data were processed using NMRPipe/NMRDraw (54) and analyzed using CCPN Analysis (55). Backbone chemical shifts for C2(C771A) and varC2(C771A) were deposited in Biological Magnetic Resonance Bank (BMRB) under accession numbers 27429 and 27430, respectively. TALOS+ (34) was used to predict C2 domain secondary structure from the assigned NMR chemical shifts. For comparison, secondary structure was pre-

dicted from crystal structures using SPARTA+ (33) to convert the coordinates to chemical shifts and then using those to predict secondary structure.

Numerous ¹H-¹⁵N HSQC-monitored titrations of C2(C771A) and one of WTC2 with CaCl₂ were conducted, including attempts to produce NMR samples that were initially calcium-free, which involved buffer solutions made with commercial calcium-free water and treatment with EGTA. Typical initial sample conditions for these experiments were 50 mM MES, pH 6.5, 50 mM NaCl, and 10 mM MES, pH 6.5, 150 mM NaCl, sometimes with EGTA (1 or 2 mM) as an additional measure to try to ensure that C2 was not Ca²⁺-bound to begin with. Final CaCl₂ concentrations in some of these titrations exceeded 15 mM, in one case reaching 76 mM.

Titrations of C2(C771A) with PI(3)P and PI(4,5)P₂ were monitored via ¹H-¹⁵N HSQC spectra recorded at Mill Hill (700-MHz cryoprobe system), and titration of varC2 with PI(4,5)P₂ was monitored via ¹H-¹⁵N HSQC spectra recorded in-house (600-MHz ambient temperature probe). Protein concentration used for these titrations was in the range 0.3–0.5 mM. DiC₄ versions of phosphoinositides (Echelon Biosciences) were used in these NMR experiments and in XRC (described below). The molar ratio of C2 to diC₄-phosphoinositide at each titration point was 1:0, 1:0.25, 1:0.50, 1:0.75, 1:1, and 1:1.5 (phosphoinositide cost-prohibited higher phosphoinositide levels); a ¹H-¹⁵N-HSQC spectrum was recorded at each titration point. CaCl₂ was then titrated into the same NMR sample with ratios of C2 to CaCl₂ of 1:0.25, 1:0.50, 1:0.75, and 1:1; a ¹H-¹⁵N-HSQC spectrum was recorded after each CaCl₂ addition. ¹H-¹⁵N chemical shift changes are reported as $\Delta\delta_{av}$ (ppm) where $\Delta\delta_{av}$ (ppm) = $((\Delta\delta_H^2 + \Delta\delta_N^2(\gamma_N/\gamma_H))/2)^{0.5}$ (56).

Analytical ultracentrifugation

Sedimentation velocity scans were recorded for four (varC2) or five (WTC2, C2(C771A), and varC2(C771A)) concentrations of each construct; concentrations are listed in each panel of Fig. S1. All experiments were performed at 50,000 rpm using a Beckman XL-I analytical ultracentrifuge with an An-50Ti rotor. Data were recorded using the absorbance (at 280 nm) and interference optical detection systems. The density and viscosity of the buffers were measured using a DMA 5000M densitometer equipped with a Lovis 200ME viscometer module. The partial specific volume for each protein was calculated using Sednterp from the amino acid sequence. Data were processed using SEDFIT (57), fitting to the *c*(s) model (Table S2).

X-ray crystallography

Crystallization was performed using ProPlex and JCSG+ screens (Molecular Dimensions), utilizing the hanging drop vapor diffusion method at 18 °C. VarC2 crystallized in 0.15 M (NH₄)₂SO₄, 0.1 M MES, pH 6.0, 15% (w/v) PEG 4000; C2(C771A) (no ligand) crystallized in 0.1 M Na-HEPES, pH 7.5, 0.8 M NaH₂PO₄, 0.8 M KH₂PO₄; and for the lipid-bound studies, the NMR samples containing ligand were crystallized in 0.1 M Tris, pH8.0, 1.5 M (NH₄)₂SO₄. Glycerol was used as a cryoprotectant at 25% (v/v) for all but the C2(C771A) (no ligand) crystals where 5% was sufficient. Diffraction data were collected

KIBRA C2: Distinctive phosphoinositide and Ca²⁺ binding

using a Rigaku MicroMax 007HF with a Saturn 944+ charge-coupled device detector. Data were processed with D*Trek or HKL-2000 (58). Molecular replacement was carried out with BALBES (59), and the model was refined using Coot (60) and PHENIX (61). The resultant structures were evaluated using MolProbity (62, 63). Data collection and processing statistics are given in Table S4.

Coarse-grained molecular dynamics (CG-MD) simulations

CG-MD simulations were performed using the Martini 2.1 force field (64, 65) and GROMACS (66). In the CG-MD simulations, the protein (in monomeric and dimeric forms) was displaced away from a preformed bilayer. Protein orientation relative to the bilayer was different at the beginning of each repeat simulation. 25 repeat simulations of 2 μ s each were conducted. The bilayer consisted of 1-palmitoyl-2-oleoyl-*sn*-glycero-3-phosphocholine (~73%), 1-palmitoyl-2-oleoyl-*sn*-glycero-3-phosphoserine (~20%), PI(4,5)P₂ (~5%), and PI(3,4,5)P₃ (~2%). All systems were energy-minimized and subsequently equilibrated (for 500 ns) with the protein backbone particle restrained. For the production simulation, the time step was 20 fs, the pressure was 1 bar, and the temperature was 323 K. Berendsen's algorithm (67) was used to control the pressure and temperature. An elastic network model was applied to all backbone particles with a cutoff distance of 0.7 nm (68). The LINCS algorithm was used to constrain bond lengths (69), and the Lennard-Jones interactions were shifted to zero between 0.9 and 1.2 nm. Coulombic interactions were shifted to zero between 0 and 1.2 nm.

Atomistic MD simulations

Atomistic MD simulations were run at 310 K using GROMACS and two different force fields: the GROMOS96 43a1 force field (70) was used with SPC water molecules, and the OPLS-AA force field was used with TIP4P water molecules. The velocity rescaling method (71) was used to control the temperature, and the Parrinello-Rahman barostat (72) was used for pressure control. Isotropic pressure coupling was used. Bond lengths were constrained to equilibrium lengths using the LINCS method, and the particle mesh Ewald method was used to model the electrostatic interactions. The time step was 2 fs. WTC2, varC2, and varC2(C771A) structures were used for these simulations. Two simulations of 100 ns and one simulation of 300 ns were performed for each force field. We also performed simulations conducted with monomeric KIBRA C2 domain in solution in which eight calcium ions were randomly added. Eight repeat 100-ns simulations were performed, each starting from different initial configurations, using the OPLS-AA force field with TIP4P water molecules.

Author contributions—M. G. P., A. U., R. I., A. C. K., G. H., S. J. C., and S. B. formal analysis; M. G. P., A. U., R. I., A. C. K., G. H., S. J. C., and S. B. investigation; M. G. P., A. U., R. I., A. C. K., and S. B. methodology; M. G. P., A. U., R. I., A. C. K., G. H., J. K., M. S. S., S. J. C., and S. B. writing-review and editing; J. K. resources; M. S. S. software; M. S. S., S. J. C., and S. B. supervision; S. B. conceptualization; S. B. funding acquisition; S. B. writing-original draft; S. B. project administration.

Acknowledgments—We are very grateful to Geoff Kelly and Alain Oregioni, Medical Research Council Biomedical NMR Centre, Mill Hill (now Crick Institute) and Christina Redfield, Department of Biochemistry, University of Oxford, for kind assistance with NMR data acquisition.

References

1. Rayala, S. K., den Hollander, P., Manavathi, B., Talukder, A. H., Song, C., Peng, S., Barnekow, A., Kremerskothen, J., and Kumar, R. (2006) Essential role of KIBRA in co-activator function of dynein light chain 1 in mammalian cells. *J. Biol. Chem.* **281**, 19092–19099 [CrossRef Medline](#)
2. Zhang, L., Yang, S., Wennmann, D. O., Chen, Y., Kremerskothen, J., and Dong, J. (2014) KIBRA: in the brain and beyond. *Cell. Signal.* **26**, 1392–1399 [CrossRef Medline](#)
3. Corneveaux, J. J., Liang, W. S., Reiman, E. M., Webster, J. A., Myers, A. J., Zismann, V. L., Joshipura, K. D., Pearson, J. V., Hu-Lince, D., Craig, D. W., Coon, K. D., Duncley, T., Bandy, D., Lee, W., Chen, K., *et al.* (2010) Evidence for an association between KIBRA and late-onset Alzheimer's disease. *Neurobiol. Aging* **31**, 901–909 [CrossRef Medline](#)
4. Tracy, T. E., Sohn, P. D., Minami, S. S., Wang, C., Min, S.-W., Li, Y., Zhou, Y., Le, D., Lo, I., Ponnusamy, R., Cong, X., Schilling, B., Ellerby, L. M., Haganir, R. L., and Gan, L. (2016) Acetylated tau obstructs KIBRA-mediated signaling in synaptic plasticity and promotes tauopathy-related memory loss. *Neuron* **90**, 245–260 [CrossRef Medline](#)
5. Ling, J., Huang, Y., Zhang, L., Wei, D., and Cheng, W. (2018) Association of KIBRA polymorphism with risk of Alzheimer's disease: evidence based on 20 case-control studies. *Neurosci. Lett.* **662**, 77–83 [CrossRef Medline](#)
6. Meliandro, K., Wong, J. S., Ray, J., Calizo, R. C., Towne, S., Cole, B., El Salem, F., Gordon, R. E., Kaufman, L., He, J. C., Azeloglu, E. U., and Campbell, K. N. (2017) The Hippo pathway regulator KIBRA promotes podocyte injury by inhibiting YAP signaling and disrupting actin cytoskeletal dynamics. *J. Biol. Chem.* **292**, 21137–21148 [CrossRef Medline](#)
7. Willsey, A. J., Fernandez, T. V., Yu, D., King, R. A., Dietrich, A., Xing, J., Sanders, S. J., Mandell, J. D., Huang, A. Y., Richer, P., Smith, L., Dong, S., Samocha, K. E., Tourette International Collaborative Genetics (TIC Genetics), Tourette Syndrome Association International Consortium for Genetics (TSAICG), *et al.* (2017) *De novo* coding variants are strongly associated with Tourette Disorder. *Neuron* **94**, 486.e9–499.e9 [CrossRef Medline](#)
8. Wilson, K. E., Yang, N., Mussell, A. L., and Zhang, J. (2016) The regulatory role of KIBRA and PTPN14 in Hippo signaling and beyond. *Genes* **7**, E23 [CrossRef Medline](#)
9. Hermann, A., Wennmann, D. O., Gromnitsa, S., Edeling, M., Van Marck, V., Sudol, M., Schaefer, L., Duning, K., Weide, T., Pavenstädt, H., and Kremerskothen, J. (2018) WW and C2 domain-containing proteins regulate hepatic cell differentiation and tumorigenesis through the hippo signaling pathway. *Hepatology* **67**, 1546–1559 [CrossRef Medline](#)
10. Wennmann, D. O., Schmitz, J., Wehr, M. C., Krahn, M. P., Koschmal, N., Gromnitsa, S., Schulze, U., Weide, T., Chekuri, A., Skryabin, B. V., Gerke, V., Pavenstädt, H., Duning, K., and Kremerskothen, J. (2014) Evolutionary and molecular facts link the WWC protein family to Hippo signaling. *Mol. Biol. Evol.* **31**, 1710–1723 [CrossRef Medline](#)
11. Yoshihama, Y., Hirai, T., Ohtsuka, T., and Chida, K. (2009) KIBRA co-localizes with protein kinase M ζ (PKM ζ) in the mouse hippocampus. *Biochem. Biotechnol. Biochem.* **73**, 147–151 [CrossRef Medline](#)
12. Yoshihama, Y., Sasaki, K., Horikoshi, Y., Suzuki, A., Ohtsuka, T., Hakuno, F., Takahashi, S., Ohno, S., and Chida, K. (2011) KIBRA suppresses apical exocytosis through inhibition of aPKC kinase activity in epithelial cells. *Curr. Biol.* **21**, 705–711 [CrossRef Medline](#)
13. Duning, K., Schurek, E. M., Schlüter, M., Bayer, M., Reinhardt, H. C., Schwab, A., Schaefer, L., Benzing, T., Schermer, B., Saleem, M. A., Huber, T. B., Bachmann, S., Kremerskothen, J., Weide, T., and Pavenstädt, H. (2008) KIBRA modulates directional migration of podocytes. *J. Am. Soc. Nephrol.* **19**, 1891–1903 [CrossRef Medline](#)

14. Rosse, C., Formstecher, E., Boeckeler, K., Zhao, Y., Kremerskothen, J., White, M. D., Camonis, J. H., and Parker, P. J. (2009) An aPKC-Exocyst complex controls Paxillin phosphorylation and migration through localized JNK1 activation. *PLoS Biol.* **7**, e1000235 [CrossRef Medline](#)
15. Papassotiropoulos, A., Stephan, D. A., Huentelman, M. J., Hoerndli, F. J., Craig, D. W., Pearson, J. V., Huynh, K. D., Brunner, F., Corneveaux, J., Osborne, D., Wollmer, M. A., Aerni, A., Coluccia, D., Hänggi, J., Mondadori, *et al.* (2006) Common Kibra alleles are associated with human memory performance. *Science* **314**, 475–478 [CrossRef Medline](#)
16. Milnik, A., Heck, A., Vogler, C., Heinze, H.-J., de Quervain, D. J. F., and Papassotiropoulos, A. (2012) Association of KIBRA with episodic and working memory: a meta-analysis. *Am. J. Med. Genet. B Neuropsychiatr. Genet.* **159B**, 958–969 [CrossRef Medline](#)
17. Kawai, E., Shibata, N., Nagata, T., Shinagawa, S., Tagai, K., Ohnuma, T., Shimazaki, H., Toda, A., Kasanuki, K., Takayama, T., Suzuki, A., Nakayama, K., Yamada, H., and Arai, H. (2015) Genetic association between KIBRA polymorphism and Alzheimer's disease within a Japanese population. *Neuromolecular Med.* **17**, 170–177 [CrossRef Medline](#)
18. Zhang, N., Liu, H., Qin, W., Liu, B., Jiang, T., and Yu, C. (2017) APOE and KIBRA interactions on brain functional connectivity in healthy young adults. *Cereb. Cortex* **27**, 4797–4805 [CrossRef Medline](#)
19. Piras, I. S., Krate, J., Schrauwen, I., Corneveaux, J. J., Serrano, G. E., Sue, L., Beach, T. G., and Huentelman, M. J. (2017) Whole transcriptome profiling of the human hippocampus suggests an involvement of the KIBRA rs17070145 polymorphism in differential activation of the MAPK signaling pathway. *Hippocampus* **27**, 784–793 [CrossRef Medline](#)
20. Johannsen, S., Duning, K., Pavenstädt, H., Kremerskothen, J., and Boeckers, T. M. (2008) Temporal-spatial expression and novel biochemical properties of the memory-related protein KIBRA. *Neuroscience* **155**, 1165–1173 [CrossRef Medline](#)
21. Schneider, A., Huentelman, M. J., Kremerskothen, J., Duning, K., Spoelgen, R., and Nikolich, K. (2010) KIBRA: a new gateway to learning and memory? *Front. Aging Neurosci.* **2**, 4 [CrossRef Medline](#)
22. Sacktor, T. C. (2011) How does PKM ζ maintain long-term memory? *Nat. Rev. Neurosci.* **12**, 9–15 [CrossRef Medline](#)
23. Büther, K., Plaas, C., Barnekow, A., and Kremerskothen, J. (2004) KIBRA is a novel substrate for protein kinase C ζ . *Biochem. Biophys. Res. Commun.* **317**, 703–707 [CrossRef Medline](#)
24. Makuch, L., Volk, L., Anggono, V., Johnson, R. C., Yu, Y., Duning, K., Kremerskothen, J., Xia, J., Takamiya, K., and Huganir, R. L. (2011) Regulation of AMPA receptor function by the human memory-associated gene KIBRA. *Neuron* **71**, 1022–1029 [CrossRef Medline](#)
25. Vogt-Eisele, A., Krüger, C., Duning, K., Weber, D., Spoelgen, R., Pitzer, C., Plaas, C., Eisenhardt, G., Meyer, A., Vogt, G., Krieger, M., Handwerker, E., Wennmann, D. O., Weide, T., Skryabin, B. V., *et al.* (2014) KIBRA (Kidney/BRain protein) regulates learning and memory and stabilizes protein kinase M ζ . *J. Neurochem.* **128**, 686–700 [CrossRef Medline](#)
26. Kremerskothen, J., Plaas, C., Büther, K., Finger, I., Veltel, S., Matanis, T., Liedtke, T., and Barnekow, A. (2003) Characterization of KIBRA, a novel WW domain-containing protein. *Biochem. Biophys. Res. Commun.* **300**, 862–867 [CrossRef Medline](#)
27. Kremerskothen, J., Plaas, C., Kindler, S., Frotscher, M., and Barnekow, A. (2005) Synaptopodin, a molecule involved in the formation of the dendritic spine apparatus, is a dual actin/ α -actinin binding protein. *J. Neurochem.* **92**, 597–606 [CrossRef Medline](#)
28. Tracy, T. E., and Gan, L. (2017) Acetylated tau in Alzheimer's disease: an instigator of synaptic dysfunction underlying memory loss: increased levels of acetylated tau blocks the postsynaptic signaling required for plasticity and promotes memory deficits associated with tauopathy. *BioEssays* **39** [CrossRef Medline](#)
29. Heitz, F. D., Farinelli, M., Mohanna, S., Kahn, M., Duning, K., Frey, M. C., Pavenstädt, H., and Mansuy, I. M. (2016) The memory gene KIBRA is a bidirectional regulator of synaptic and structural plasticity in the adult brain. *Neurobiol. Learn. Mem.* **135**, 100–114 [CrossRef Medline](#)
30. Duning, K., Wennmann, D. O., Bokemeyer, A., Reissner, C., Wersching, H., Thomas, C., Buschert, J., Guske, K., Franzke, V., Flöel, A., Lohmann, H., Knecht, S., Brand, S.-M., Pöter, M., Rescher, U., *et al.* (2013) Common exonic missense variants in the C2 domain of the human KIBRA protein modify lipid binding and cognitive performance. *Transl. Psychiatry* **3**, e272 [CrossRef Medline](#)
31. Corbalán-García, S., and Gómez-Fernández, J. C. (2014) Signaling through C2 domains: more than one lipid target. *Biochim. Biophys. Acta* **1838**, 1536–1547 [CrossRef Medline](#)
32. Lemmon, M. A. (2008) Membrane recognition by phospholipid-binding domains. *Nat. Rev. Mol. Cell Biol.* **9**, 99–111 [CrossRef Medline](#)
33. Shen, Y., and Bax, A. (2010) SPARTA+: a modest improvement in empirical NMR chemical shift prediction by means of an artificial neural network. *J. Biomol. NMR* **48**, 13–22 [CrossRef Medline](#)
34. Shen, Y., Delaglio, F., Cornilescu, G., and Bax, A. (2009) TALOS+: a hybrid method for predicting protein backbone torsion angles from NMR chemical shifts. *J. Biomol. NMR* **44**, 213–223 [CrossRef Medline](#)
35. Yamamoto, E., Kalli, A. C., Yasuoka, K., and Sansom, M. S. P. (2016) Interactions of pleckstrin homology domains with membranes: adding back the bilayer via high-throughput molecular dynamics. *Structure* **24**, 1421–1431 [CrossRef Medline](#)
36. Kalli, A. C., and Sansom, M. S. (2014) Interactions of peripheral proteins with model membranes as viewed by molecular dynamics simulations. *Biochem. Soc. Trans.* **42**, 1418–1424 [CrossRef Medline](#)
37. Khanal, P., Jia, Z., and Yang, X. (2018) Cysteine residues are essential for dimerization of Hippo pathway components YAP2L and TAZ. *Sci. Rep.* **8**, 3485 [CrossRef Medline](#)
38. Cumming, R. C., Andon, N. L., Haynes, P. A., Park, M., Fischer, W. H., and Schubert, D. (2004) Protein disulfide bond formation in the cytoplasm during oxidative stress. *J. Biol. Chem.* **279**, 21749–21758 [CrossRef Medline](#)
39. Ashraf, A., and Pervaiz, S. (2015) Hippo circuitry and the redox modulation of hippo components in cancer cell fate decisions. *Int. J. Biochem. Cell Biol.* **69**, 20–28 [CrossRef Medline](#)
40. Cheignon, C., Tomas, M., Bonnefont-Rousselot, D., Faller, P., Hureau, C., and Collin, F. (2018) Oxidative stress and the amyloid beta peptide in Alzheimer's disease. *Redox Biol.* **14**, 450–464 [CrossRef Medline](#)
41. Ubach, J., Lao, Y., Fernandez, I., Arac, D., Südhof, T. C., and Rizo, J. (2001) The C2B domain of synaptotagmin I is a Ca²⁺-binding module. *Biochemistry* **40**, 5854–5860 [CrossRef Medline](#)
42. Voskoboinik, I., Thia, M.-C., Fletcher, J., Ciccone, A., Browne, K., Smyth, M. J., and Trapani, J. A. (2005) Calcium-dependent plasma membrane binding and cell lysis by perforin are mediated through its C2 domain. *J. Biol. Chem.* **280**, 8426–8434 [CrossRef Medline](#)
43. Ubach, J., García, J., Nittler, M. P., Südhof, T. C., and Rizo, J. (1999) Structure of the Janus-faced C2B domain of rabphilin. *Nat. Cell Biol.* **1**, 106–112 [CrossRef Medline](#)
44. Montaville, P., Schlicker, C., Leonov, A., Zweckstetter, M., Sheldrick, G. M., and Becker, S. (2007) The C2A-C2B linker defines the high affinity Ca²⁺ binding mode of rabphilin-3A. *J. Biol. Chem.* **282**, 5015–5025 [CrossRef Medline](#)
45. Dai, H., Shin, O.-H., Machius, M., Tomchick, D. R., Südhof, T. C., and Rizo, J. (2004) Structural basis for the evolutionary inactivation of Ca²⁺ binding to synaptotagmin 4. *Nat. Struct. Mol. Biol.* **11**, 844–849 [CrossRef Medline](#)
46. Verdaguer, N., Corbalán-García, S., Ochoa, W. F., Fita, I., and Gómez-Fernández, J. C. (1999) Ca²⁺ bridges the C2 membrane-binding domain of protein kinase C α directly to phosphatidylserine. *EMBO J.* **18**, 6329–6338 [CrossRef Medline](#)
47. Guerrero-Valero, M., Ferrer-Orta, C., Querol-Audí, J., Marin-Vicente, C., Fita, I., Gómez-Fernández, J. C., Verdaguer, N., and Corbalán-García, S. (2009) Structural and mechanistic insights into the association of PKC-C2 domain to Ptdins(4,5)P2. *Proc. Natl. Acad. Sci. U.S.A.* **106**, 6603–6607 [CrossRef Medline](#)
48. Ochoa, W. F., Corbalán-García, S., Eritja, R., Rodríguez-Alfaro, J. A., Gómez-Fernández, J. C., Fita, I., and Verdaguer, N. (2002) Additional binding sites for anionic phospholipids and calcium ions in the crystal structures of complexes of the C2 domain of protein kinase C α . *J. Mol. Biol.* **320**, 277–291 [CrossRef Medline](#)
49. Ferrer-Orta, C., Pérez-Sánchez, M. D., Coronado-Parra, T., Silva, C., López-Martínez, D., Baltanás-Copado, J., Gómez-Fernández, J. C., Corbalán-García, S., and Verdaguer, N. (2017) Structural characterization of the

KIBRA C2: Distinctive phosphoinositide and Ca²⁺ binding

- Rabphilin-3A-SNAP25 interaction. *Proc. Natl. Acad. Sci. U.S.A.* **114**, E5343–E5351 [CrossRef Medline](#)
50. Coudeville, N., Montaville, P., Leonov, A., Zweckstetter, M., and Becker, S. (2008) Structural determinants for Ca²⁺ and phosphatidylinositol 4,5-bisphosphate binding by the C2A domain of rabphilin-3A. *J. Biol. Chem.* **283**, 35918–35928 [CrossRef Medline](#)
51. Montaville, P., Coudeville, N., Radhakrishnan, A., Leonov, A., Zweckstetter, M., and Becker, S. (2008) The PIP2 binding mode of the C2 domains of rabphilin-3A. *Protein Sci.* **17**, 1025–1034 [CrossRef Medline](#)
52. Picas, L., Viaud, J., Schauer, K., Vanni, S., Hnia, K., Fraiser, V., Roux, A. E. L., Bassereau, P., Gaits-Iacovoni, F., Payrastra, B., Laporte, J., Mannerville, J.-B., and Goud, B. (2014) BIN1/M-Amphiphysin2 induces clustering of phosphoinositides to recruit its downstream partner dynamin. *Nat. Commun.* **5**, 5647 [CrossRef Medline](#)
53. Posner, M. G., Upadhyay, A., Bagby, S., Hough, D. W., and Danson, M. J. (2009) A unique lipoylation system in the Archaea. *FEBS J.* **276**, 4012–4022 [CrossRef Medline](#)
54. Delaglio, F., Grzesiek, S., Vuister, G. W., Zhu, G., Pfeifer, J., and Bax, A. (1995) NMRPipe: a multidimensional spectral processing system based on UNIX pipes. *J. Biomol NMR* **6**, 277–293 [Medline](#)
55. Vranken, W. F., Boucher, W., Stevens, T. J., Fogh, R. H., Pajon, A., Llinas, M., Ulrich, E. L., Markley, J. L., Ionides, J., and Laue, E. D. (2005) The CCPN data model for NMR spectroscopy: development of a software pipeline. *Proteins* **59**, 687–696 [CrossRef Medline](#)
56. Williamson, M. P. (2013) Using chemical shift perturbation to characterise ligand binding. *Prog. Nucl. Magn. Reson. Spectrosc.* **73**, 1–16 [CrossRef Medline](#)
57. Schuck, P. (2000) Size-distribution analysis of macromolecules by sedimentation velocity ultracentrifugation and Lamm equation modeling. *Biophys. J.* **78**, 1606–1619 [CrossRef Medline](#)
58. Otwinowski, Z., and Minor, W. (1997) Processing of X-ray diffraction data collected in oscillation mode. *Methods Enzymol.* **276**, 307–326 [CrossRef Medline](#)
59. Long, F., Vagin, A. A., Young, P., and Murshudov, G. N. (2008) BALBES: a molecular-replacement pipeline. *Acta Crystallogr. D Biol. Crystallogr.* **64**, 125–132 [CrossRef Medline](#)
60. Emsley, P., Lohkamp, B., Scott, W. G., and Cowtan, K. (2010) Features and development of Coot. *Acta Crystallogr. D Biol. Crystallogr.* **66**, 486–501 [CrossRef Medline](#)
61. Adams, P. D., Afonine, P. V., Bunkóczi, G., Chen, V. B., Davis, I. W., Echols, N., Headd, J. J., Hung, L. W., Kapral, G. J., Grosse-Kunstleve, R. W., McCoy, A. J., Moriarty, N. W., Oeffner, R., Read, R. J., Richardson, D. C., et al. (2010) PHENIX: a comprehensive Python-based system for macromolecular structure solution. *Acta Crystallogr. D Biol. Crystallogr.* **66**, 213–221 [CrossRef Medline](#)
62. Davis, I. W., Leaver-Fay, A., Chen, V. B., Block, J. N., Kapral, G. J., Wang, X., Murray, L. W., Arendall, W. B., 3rd, Snoeyink, J., Richardson, J. S., and Richardson, D. C. (2007) MolProbity: all-atom contacts and structure validation for proteins and nucleic acids. *Nucleic Acids Res.* **35**, W375–W383 [CrossRef Medline](#)
63. Chen, V. B., Arendall, W. B., Headd, J. J., Keedy, D. A., Immormino, R. M., Kapral, G. J., Murray, L. W., Richardson, J. S., and Richardson, D. C. (2010) MolProbity: all-atom structure validation for macromolecular crystallography. *Acta Crystallogr. D Biol. Crystallogr.* **66**, 12–21 [CrossRef Medline](#)
64. Marrink, S. J., Risselada, H. J., Yefimov, S., Tieleman, D. P., and de Vries, A. H. (2007) The MARTINI force field: coarse grained model for biomolecular simulations. *J. Phys. Chem. B* **111**, 7812–7824 [CrossRef Medline](#)
65. Monticelli, L., Kandasamy, S. K., Periole, X., Larson, R. G., Tieleman, D. P., and Marrink, S.-J. (2008) The MARTINI coarse-grained force field: extension to proteins. *J. Chem. Theory Comput.* **4**, 819–834 [CrossRef Medline](#)
66. Hess, B., Kutzner, C., van der Spoel, D., and Lindahl, E. (2008) GROMACS 4: algorithms for highly efficient, load-balanced, and scalable molecular simulation. *J. Chem. Theory Comput.* **4**, 435–447 [CrossRef Medline](#)
67. Berendsen, H. J. C., Postma, J. P. M., van Gunsteren, W. F., DiNola, A., and Haak, J. R. (1984) Molecular dynamics with coupling to an external bath. *J. Chem. Phys.* **81**, 3684–3690 [CrossRef](#)
68. Atilgan, A. R., Durell, S. R., Jernigan, R. L., Demirel, M. C., Keskin, O., and Bahar, I. (2001) Anisotropy of fluctuation dynamics of proteins with an elastic network model. *Biophys. J.* **80**, 505–515 [CrossRef Medline](#)
69. Hess, B., Bekker, H., Berendsen, H. J. C., Fraaije, J. G. E. M. (1997) LINC: a linear constraint solver for molecular simulations. *J. Comput. Chem.* **18**, 1463–1472 [CrossRef](#)
70. Scott, W. R. P., Hünenberger, P. H., Tironi, I. G., Mark, A. E., Billeter, S. R., Fennen, J., Torda, A. E., Huber, T., Krüger, P., and van Gunsteren, W. F. (1999) The GROMOS biomolecular simulation program package. *J. Phys. Chem. A* **103**, 3596–3607 [CrossRef](#)
71. Bussi, G., Donadio, D., and Parrinello, M. (2007) Canonical sampling through velocity rescaling. *J. Chem. Phys.* **126**, 014101–014108 [CrossRef Medline](#)
72. Parrinello, M., and Rahman, A. (1981) Polymorphic transitions in single crystals: A new molecular dynamics method. *J. Appl. Phys.* **52**, 7182–7190 [CrossRef](#)

Distinctive phosphoinositide- and Ca²⁺-binding properties of normal and cognitive performance –linked variant forms of KIBRA C2 domain

Mareike G. Posner, Abhishek Upadhyay, Rieko Ishima, Antreas C. Kalli, Gemma Harris, Joachim Kremerskothen, Mark S. P. Sansom, Susan J. Crennell and Stefan Bagby

J. Biol. Chem. 2018, 293:9335-9344.

doi: 10.1074/jbc.RA118.002279 originally published online May 3, 2018

Access the most updated version of this article at doi: [10.1074/jbc.RA118.002279](https://doi.org/10.1074/jbc.RA118.002279)

Alerts:

- [When this article is cited](#)
- [When a correction for this article is posted](#)

[Click here](#) to choose from all of JBC's e-mail alerts

This article cites 72 references, 12 of which can be accessed free at <http://www.jbc.org/content/293/24/9335.full.html#ref-list-1>